Applied Catalysis B: Environmental 140–141 (2013) 60–67

Contents lists available at SciVerse ScienceDirect

Applied Catalysis B: Environmental

journal homepage: www.elsevier.com/locate/apcatb

Alkaline metals modified Pt–$H_4SiW_{12}O_{40}/ZrO_2$ catalysts for the selective hydrogenolysis of glycerol to 1,3-propanediol

Shanhui Zhu[a,b], Xiaoqing Gao[c], Yulei Zhu[a,c,*], Yifeng Zhu[a,b], Xiaomin Xiang[a,b], Caixia Hu[c], Yongwang Li[a,c]

[a] State Key Laboratory of Coal Conversion, Institute of Coal Chemistry, Chinese Academy of Sciences, Taiyuan 030001, PR China
[b] Graduate University of Chinese Academy of Sciences, Beijing 100039, PR China
[c] Synfuels China Co. Ltd., Taiyuan 030032, PR China

ARTICLE INFO

Article history:
Received 28 December 2012
Received in revised form 25 March 2013
Accepted 27 March 2013
Available online 2 April 2013

Keywords:
Glycerol
Hydrogenolysis
1,3-Propanediol
Alkaline metals
Silicotungstic acid

ABSTRACT

Catalytic hydrogenolysis of glycerol to value-added 1,3-propanediol (1,3-PDO) holds the potential to utilize the large surplus of crude glycerol from biodiesel industry. A series of alkaline metals (Li, K, Rb and Cs) modified Pt–$H_4SiW_{12}O_{40}/ZrO_2$ catalysts were prepared, characterized and evaluated for this reaction. The bulk and surface features of these catalysts were characterized by several techniques, including BET, CO-chemisorption, XRD, Raman, SEM-EDX, NH_3-TPD and FTIR of adsorbed pyridine. Among them, Li exchanged $H_4SiW_{12}O_{40}$ (HSiW) exhibited superior activity and maximum 1,3-PDO selectivity due to the enhanced Brønsted acid sites. This catalyst achieved 120 h long-term stability owing to the strong interaction of active components with ZrO_2, remaining of unique Keggin structure as well as the enhanced water-tolerance. There is a linear relationship between 1,3-PDO yield and concentration of Brønsted acid sites, providing direct evidence that Brønsted acid sites are responsible for the selective formation of 1,3-PDO from glycerol hydrogenolysis.

1. Introduction

The utilization of renewable biomass provides a facile route to alleviate the shortage of fossil fuels and reduce CO_2 emission [1,2]. Being a biomass-derivate, glycerol is currently produced from biodiesel process which brings a huge amount of glycerol close to 10 wt% of the overall biodiesel production [3,4]. Nowadays, a large surplus of crude glycerol is burned directly, which must be considered as a tragic waste of a potentially versatile raw material [5]. Thus, significant work [3,4,6–9] has been devoted to the transformation of low-cost glycerol into value-added chemicals. In this context, hydrogenolysis of glycerol to 1,3-propanediol (1,3-PDO) and 1,2-propanediol (1,2-PDO) is one of the most promising sustainable processes to valorize surplus glycerol due to their versatile applications as intermediates in the synthesis of many fine chemicals [4,6]. In contrast to tremendous efforts focused on conversion of glycerol to 1,2-PDO, the available reports dealing with the potential transformation of glycerol for synthesis of 1,3-PDO are limited. 1,3-PDO is much more valuable than 1,2-PDO, particularly as an important monomer to produce high performance biodegradable polyesters [6]. Additionally, high 1,2-PDO yields in glycerol hydrogenolysis have been achieved and the first commercial plant with a capacity of 0.1 million tons 1,2-PDO from biodiesel glycerol has been opened [4]. Nevertheless, hydrogenolysis of glycerol to 1,3-PDO is still a challenge wherein the urgent problem is how to cleave C—O bond selectively.

It is well-known that hydrogenolysis of glycerol to 1,3-PDO involved dehydration of glycerol to 3-hydroxypropaldehyde (3-HPA) on acidic sites followed by subsequent hydrogenation on metal center [10,11]. Thus, the appropriate combination of metal components and acidic species in reaction system is indispensable for the effective formation of 1,3-PDO. The relatively feasible hydrogenolysis processes that have been reported employed $Pt/WO_3/ZrO_2$ [12,13], $Rh/SiO_2 + H_2WO_4$ [14], $Pt/WO_3/TiO_2/SiO_2$ [15], Pt–sulfated zirconia [16], $Ir–ReO_x/SiO_2 + H_2SO_4$ [17,18] as catalysts. Most of previous studies have been performed in organic solvent or with liquid acids, which will greatly reduce environmental and economical viability. To address these problems, recently we have developed a continuous process for glycerol hydrogenolysis to 1,3-PDO over ZrO_2 and SiO_2 supported Pt–HSiW bifunctional catalysts using water as solvent, which provided a sustainable and economical reaction system [11,19]. These results show that Brønsted acid sites appear as a key to the selective formation of 1,3-PDO, but the surface reaction mechanism is still not unclear.

* Corresponding author at: State Key Laboratory of Coal Conversion, Institute of Coal Chemistry, Chinese Academy of Sciences, Taiyuan 030001, PR China.
Tel.: +86 351 7117097; fax: +86 351 7560668.
E-mail address: zhuyulei@sxicc.ac.cn (Y. Zhu).

0926-3373/$ – see front matter © 2013 Elsevier B.V. All rights reserved.
http://dx.doi.org/10.1016/j.apcatb.2013.03.041

Meanwhile, the leaching problems of supported heteropolyacids (HPAs) in polar water environment need to be addressed.

Compared to conventional solid acid catalysts such as oxides or zeolites, heteropolyacids (HPAs) possess strong Brønsted acidity, uniform acid sites and easily tunable acidity, but they are highly soluble in polar media [20–22]. Although HPAs grafting onto porous supports can improve their dispersion and accessible acid sites, this cannot wholly overcome the solubility issue in polar medium [23]. Oliveira et al. [24] have found that about 8.0 wt% tungstophosphoric acid (HPW) was leached at the second cycle test in esterification of oleic acid with ethanol over HPW/ZrO_2 catalyst. Alkali exchanged HPAs showed enhanced surface areas, outstanding water-tolerance and acidity changes relative to the bulk compound, which was another powerful tool to adjust acidic properties of HPAs [25,26]. Partially Cs^+ exchanged $Cs_{2.5}H_{0.5}PW_{12}O_{40}$ salt even presented much higher acidity than the parent HPW acid owing to the presence of residual protons capable of mobilizing and inducing new acid sites. Furthermore, alkali exchanged HPAs can significantly decline solubility in polar media and improve the stability; for example, HPAs salts with monovalent ions such as Cs^+ are insoluble in water. Narasimharao et al. [26] have claimed that the Cs-doped HPW catalysts were easily recoverable with no leaching of soluble HPW for biodiesel production. Recently, Atia et al. [27] investigated a series of Li, K and Cs modified HSiW catalysts for glycerol dehydration, which greatly improved the desired acrolein selectivity and activity. Generally, the incorporation of alkaline metals into HPAs can strengthen the water-tolerance and simultaneously adjust the acidity, resulting in increased activity and stability, particularly in polar water medium.

Herein, we investigated the potential of alkaline metals Li, K, Rb and Cs to control acidic properties of Pt–HSiW/ZrO_2 catalysts. The catalysts were examined in glycerol hydrogenolysis with the intention of exploring correlations between 1,3-PDO yield and surface acidic properties to better understand reaction mechanism, which could facilitate to develop more efficient solid acid catalysts for sustainable utilization of glycerol. Additionally, the long-term performance of preferred Li modified Pt–HSiW/ZrO_2 catalyst was also checked.

2. Experimental

2.1. Catalyst preparation

The Pt–HSiW/ZrO_2 was prepared by sequential impregnation method, which was prepared similarly according to the method described elsewhere [19,28]. At first, Pt/ZrO_2 was prepared by the impregnation of ZrO_2 (Jiangsu Qianye Co., Ltd, China) with an aqueous solution of $H_2PtCl_6{\cdot}6H_2O$ (Sinopharm Chemical Reagent Co., Ltd, China, SCRC). The impregnated sample was dried overnight at 110 °C, and then calcined at 400 °C in static air for 4 h. After impregnating HSiW (SCRC) on to Pt/ZrO_2, Pt–HSiW/ZrO_2 was dried overnight at 110 °C and then calcined at 400 °C in static air for 4 h. The weight loadings of Pt and HSiW were fixed at 1% and 20% in Pt–HSiW/ZrO_2, respectively. Alkali metals (Li, K, Rb, and Cs) were doped into Pt–HSiW/ZrO_2 by an ion-exchange method. Take Li modified Pt–HSiW/ZrO_2 as an example. Pt–HSiW/ZrO_2 was dispersed in water with constant stirring. A calculated amount of $LiNO_3$ (SCRC) was added into the solution, and then the mixture was stirred for 12 h. The sample was dried overnight at 110 °C and then calcined at 400 °C in static air for 4 h. The stoichiometric ratio of alkaline metal and HSiW was set to 2, i.e., 50% of the protons in HSiW might be replaced by alkaline metal atoms. For example, the Li exchanged HSiW was $Li_2H_2SiW_{12}O_{40}$. The alkali metals modified catalysts are designated as Pt–LiSiW/ZrO_2, Pt–KSiW/ZrO_2, Pt–RbSiW/ZrO_2 and Pt–C_SSiW/ZrO_2.

2.2. Catalyst characterization

N_2 adsorption–desorption isotherms were obtained at −196 °C on a Micromeritics ASAP 2420 instrument. Prior to the measurement, the samples were degassed under vacuum for 8 h at 350 °C.

CO chemisorption was performed on Auto Chem. II2920 equipment (Mircromeritics, USA) with a TCD detector by pulse injection of pure CO at 50 °C. Before the measurements, the catalysts were in situ reduced by flowing H_2 at 200 °C for 2 h, and then purged with He for 1 h. After cooled down to 50 °C, several pluses of CO were injected at regular intervals until saturation with CO for the sample. The Pt average particle size was calculated by assuming an adsorption of one CO molecule per surface Pt atom.

Powder X-ray diffraction (XRD) patterns were conducted on a D2/max-RA X-ray diffractometer (Bruker, Germany) with Cu Kα radiation operated at 30 kV and 10 mA. The X-ray patterns were recorded in 2θ values ranging from 10° to 90° at the scanning rate of 5°/min.

Raman spectra were carried out on a LabRAM HR800 System equipped with a multichannel air cooled CCD detector at room temperature. The 532 nm of the air cooled frequency doubled Nd–Yag laser was used as the exciting source with a power of 30 MW.

Scanning Electron Microscopy (SEM) was carried out on a Quanta 400F microscope. EDX spectra were obtained employing 20 KV primary electron voltages to explore the compositions of calcined catalysts.

NH_3-TPD was carried out in the same apparatus as CO chemisorption. In a typical run, about 0.2 g sample was loaded in a U-shaped quartz tube. Prior to the measurement, the catalyst sample was pretreated in He at 350 °C for 1 h, then cooled to 100 °C and was saturated with pure NH_3 for 30 min. After being purged with He for 30 min to remove the physically adsorbed NH_3, the sample was heated from 100 °C to 700 °C at a heating rate of 10 K/min and the NH_3 desorption was monitored with a TCD detector. Then the peak area of detected TPD peak can be correlated with the amount of desorbed NH_3 on the basis of pulsed NH_3 injection experiment.

IR spectra of adsorbed pyridine (Py-IR) were recorded with a VERTEX70 (Bruker) FT-IR spectrophotometer, equipped with a deuterium triglycine sulphate (DTGS) detector. The samples were degassed in a vacuum at 300 °C for 1 h, and then exposed to the pyridine vapor after cooling down to 30 °C. The physisorbed pyridine was flushed away by evacuating for 20 min. The Py-IR spectra were then recorded at 200 °C after applying vacuum for 30 min. The quantitative analysis of Brønsted and Lewis acid sites was based on the integrated area of adsorption bands at ca. 1540 and 1450 cm^{-1}, respectively. The extinction coefficients were also determined according to our previous reports [11,19].

ICP optical emission spectroscopy (Optima2100DV, PerkinElmer) was employed to check the leaching of active components during the long-term performance test.

2.3. Catalytic reaction

Hydrogenolysis of glycerol was performed in a vertical fixed-bed reactor (i.d. 12 mm, length 600 mm) with an ice-water trap. In a typical test, 2.0 g catalyst sample (20–40 mesh) was placed in the constant temperature section of the reactor, with quartz sand packed in both ends. Prior to each test, the catalyst was in situ reduced in a stream of pure H_2 (100 ml/min) at 200 °C for 2 h. After reduction, a 10 wt.% glycerol aqueous solution at 0.03 ml/min was pumped continuously into the reactor together with a flow of 100 ml/min co-feed H_2. The generated gas and liquid products were cooled and collected in a gas–liquid separator immersed in an ice-water trap. The standard reaction conditions were 5.0 MPa, 2.0 g catalysts, 10 wt.% glycerol aqueous solution, H_2/glycerol = 137:1

Table 1
Physicochemical properties and acidities of different catalysts.

Catalyst	Surface area ($m^2\ g^{-1}$)	Pore size (nm)	Pore volume ($cm^3\ g^{-1}$)	Pt size (nm)	Pt dispersion (%)	Total acidity (mmol $NH_3/g_{cat.}$)[a]	Brønsted acidity ($\mu mol/g_{cat.}$)[b]	Lewis acidity ($\mu mol/g_{cat.}$)[b]	Total acidity ($\mu mol/g_{cat.}$)[b]
Pt–HSiW/ZrO_2	46.9	11.7	0.18	2.64	42.9	0.61	42.7	109.2	151.9
Pt–LiSiW/ZrO_2	50.5	11.6	0.19	2.71	42.0	0.65	50.5	148.0	198.5
Pt–KSiW/ZrO_2	51.8	11.5	0.20	2.70	41.8	0.33	38.7	85.5	124.2
Pt–RbSiW/ZrO_2	53.3	11.3	0.19	2.62	43.2	0.26	36.8	70.3	107.1
Pt–CsSiW/ZrO_2	53.8	11.0	0.21	2.56	44.2	0.63	45.3	145.2	190.5

[a] The amount of acid sites was determined by quantifying the desorbed NH_3 from NH_3-TPD.
[b] The amount of acid sites was determined by quantifying the desorbed pyridine from Py-IR.

(molar ratio), WHSV = 0.09 h^{-1} with four consecutive temperature set-points at 160, 180, 200 and 220 °C.

The liquid products were determined by a gas chromatography with capillary column (DB-WAX, 30 m × 0.32 mm) and FID detector. The tail gas was off-line analyzed by a gas chromatography using capillary column (OV-101, 60 m × 0.25 mm) and TCD detector. The obtained products were also identified by a GC–MS (Agilent, USA) with DB-WAX capillary column. The conversion of glycerol and selectivity of products were calculated by the following equations:

$$\text{Conversion}\ (\%) = \frac{\text{moles of glycerol (in)} - \text{moles of glycerol (out)}}{\text{moles of glycerol (in)}} \times 100$$

$$\text{Selectivity}\ (\%) = \frac{\text{moles of one product}}{\text{moles of all products}} \times 100$$

3. Results and discussion

3.1. Catalyst characterization

3.1.1. Physicochemical properties of catalysts

The textural properties derived from nitrogen physisorption isotherms and Pt dispersion determined by CO-chemisorption are presented in Table 1. Compared to supported HSiW catalyst, the BET surface area of alkaline metal modified samples presented similar BET surface area. As listed in Table 1, all the catalysts showed small Pt nanoparticles and good dispersion of Pt, suggesting that alkaline metals scarcely had impact on the dispersion of Pt, which might be attributed to the preparation procedures. When alkaline metals were introduced into the as-prepared Pt–HSiW/ZrO_2, ion-exchange reaction occurred rapidly, which did not affect the dispersion of Pt nanoparticles because they had been immobilized firmly onto ZrO_2 surface prior to reaction. The strong interaction between Pt and ZrO_2 surface can be instrumental in preventing the crystallization of Pt nanoparticles in high temperature calcination, which resulted in homogenous distribution of Pt species on ZrO_2 surface [28].

As shown in Fig. 1, the catalysts exhibited main characteristic peaks corresponding to monoclinic phase of ZrO_2 support (e.g., 24.1°, 28.3°, 31.5°, 34.3° and 49.4°) [19]. Almost no peaks of HSiW or corresponding salts were detected, most probably due to the homogeneous distribution of HSiW or its salts on the surface. Interestingly, only Rb and Cs exchanged HSiW catalysts presented weak characteristic diffraction peaks related to respective HSiW salts, revealing the remaining of intact HSiW Keggin structure and the formation of crystalline particles after doping alkaline metal ions on HSiW secondary structure. The partial substitution of HSiW protons with alkaline metal ions caused the corresponding salts more neutral and further weakened the interaction between ZrO_2 surface hydroxyl groups and HSiW molecules, which resulted in the decline of HSiW salts dispersion [27]. This effect would be most prominent for large and basic Cs and Rb doped HSiW salts which can create crystalline particles facilely and be observed by XRD. Meanwhile, there were no diffraction peaks of Pt species, implying that the Pt nanoparticles were highly dispersed on ZrO_2 surface, consistent well with the CO chemisorption results.

As illustrated in Fig. 2, the bulk HSiW exhibited Keggin structure characteristic bands at 995 cm^{-1} (stretching of W=O), 974 cm^{-1} (bending of W—O—W) and 555 cm^{-1} (bending of O—Si—O) [29]. All the catalysts displayed characteristic bands at around 995 cm^{-1} related to W=O symmetric stretching vibrations, implying the partial preservation of HSiW Keggin structure, even after exchange of

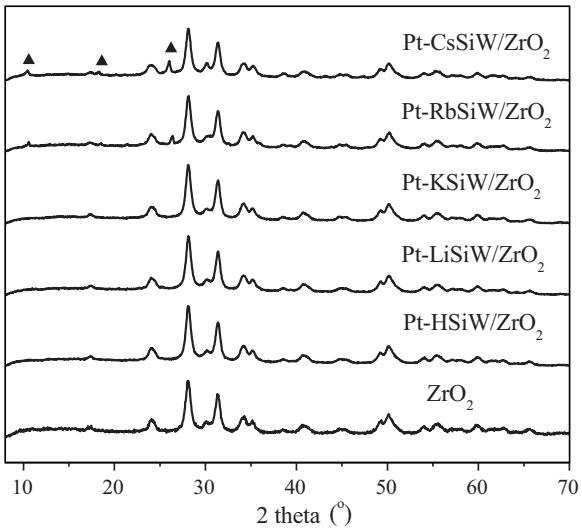

Fig. 1. XRD patterns of bulk ZrO_2, Pt–HSiW/ZrO_2 and alkaline metals modified catalysts (▲, HSiW).

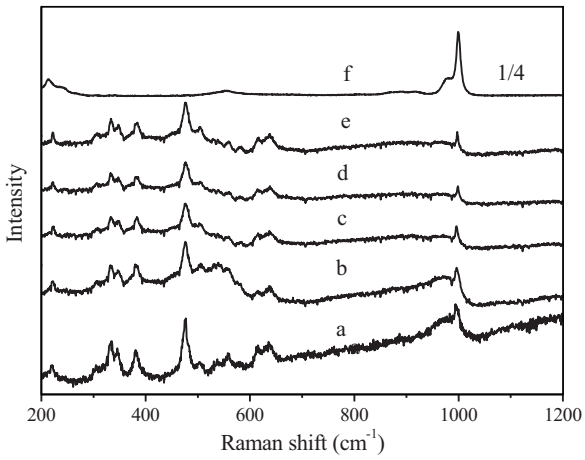

Fig. 2. Raman spectra of (a) Pt–HSiW/ZrO_2, (b) Pt–LiSiW/ZrO_2, (c) Pt–KSiW/ZrO_2, (d) Pt–RbSiW/ZrO_2, (e) Pt–CsSiW/ZrO_2 and (f) bulk HSiW.

Table 2
Energy dispersive X-ray analysis data for K, Rb, Cs and W over alkaline metals modified Pt–HSiWZrO$_2$.

Catalyst	Nominal W/alkaline metal atomic ratio	Data determined by EDX[a]	Average value from EDX
Pt–KSiW/ZrO$_2$ (W/K)	6	4.34;6.12;6.98;5.13;8.36;4.49;3.78;5.17;6.16;5.91	5.64
Pt–RbSiW/ZrO$_2$ (W/Rb)	6	5.06;4.86;5.12;5.82;5.91;5.42;7.02;6.24;6.23;7.56	5.92
Pt–CsSiW/ZrO$_2$(W/Cs)	6	4.48;5.40;4.82;5.25;6.28;8.18;4.64;7.87;8.44;6.59	6.23

[a] These data about W/alkaline metal atomic ratio was calculated on the basis of EDX analysis.

protons with alkaline metals. Nevertheless, compared with bulk HSiW, the Keggin bands of all the doped samples became weaker, broader and some of them even disappeared, which was presumably attributed to the bond weakening/distortion by strong interaction of HSiW with support and alkaline metals [19]. Addition of alkaline metal to HSiW induces a contraction effect on HSiW structure as alkaline metal replaces the $H_2O_5^+$ moieties, which can lead to the distortion of HSiW structure [30]. Accordingly, new HSiW salts were likely formed, in well agreement with the XRD results. The insoluble HSiW salts would be instrumental in preventing the leaching of HSiW components during the reaction and sustaining the long-term performance. Meanwhile, the characteristic bands of monoclinic ZrO_2 can be clearly identified, at around 337, 382, 474, 540 and 620 cm^{-1} [24].

The compositions of alkaline metal modified samples were examined by energy dispersive X-ray technique (EDX). The values about ratios of alkaline metals with W determined by EDX data are summarized in Table 2. The content of Li element over Pt–LiSiW/ZrO$_2$ cannot be detected by EDX owing to its quite light atom weight. As can be seen in Table 2, the average value from EDX was rather equivalent to the nominal ratio in the ratio of W/alkaline metals in all cases. Generally, the distribution of alkaline metals and W elements was relatively homogeneous, except that in some cases the content of W element was lower than that of nominal value, particularly for Pt–KSiW/ZrO$_2$. These observations from EDX as well as XRD results and Raman spectra confirmed that the alkaline metals were successfully incorporated into HSiW Keggin structures and formed corresponding salts.

3.1.2. Acidic properties of catalysts

It is generally accepted that the acidic properties of catalysts have significant impacts on the catalytic performance of glycerol hydrogenolysis to 1,3-PDO due to the bi-functional mechanism [31,32]. 1,3-PDO cannot be achieved effectively over those supported metal catalysts alone such as Pt/SiO$_2$ [11] and Pt/ZrO$_2$ [19] without the presence of acidic components. Accordingly, the accessible surface acidic sites of these catalysts were probed by NH$_3$-TPD and FTIR of adsorbed pyridine. Fig. 3 displays NH$_3$-TPD profiles of the as-prepared catalysts and total acidities calculated from peak areas are presented in Table 1. All the samples showed broad NH$_3$-TPD profiles, revealing that the surface acid strength is widely distributed. Pt–HSiW/ZrO$_2$ catalyst displayed a main peak and a weak shoulder, centering around 170 °C and 260 °C, respectively. The alkaline metals modification causes an increase in the strong acidic sites, whereas a decrease in the weak and moderate acidic sites was observed. This increase in strong acidic sites was related to the presence of residual protons which are mobile and capable of inducing new strong acidic sites. Similar trends have been reported in the case of Cs modified HPW and Ag exchanged silicotungstic acid catalysts [26,33]. Partially Cs^+ substituted HPW salt $Cs_{2.5}H_{0.5}PW_{12}O_{40}$ presented higher acidity than parent HPW, resulting in higher activity than parent HPW in the acid-catalyzed reactions [26]. As shown in Table 1, the total acidities of these catalysts decreased in the following order: Pt–LiSiW/ZrO$_2$ > Pt–CsSiW/ZrO$_2$ > Pt–HSiW/ZrO$_2$ > Pt–KSiW/ZrO$_2$ > Pt–RbSiW/ZrO$_2$.

The nature of acid sites was determined by FTIR spectra of pyridine adsorption (Fig. 4). The bands at around 1445 and 1610 cm^{-1} were assigned to pyridine adsorbed at Lewis acid sites [19]. The band at 1489 cm^{-1} was attributed to the combination of pyridine on Lewis acid sites and Brønsted acid sites while the absorption around 1540 cm^{-1} was typical pyridine band coordinated to Brønsted acid sites, as well as the band at 1640 cm^{-1}

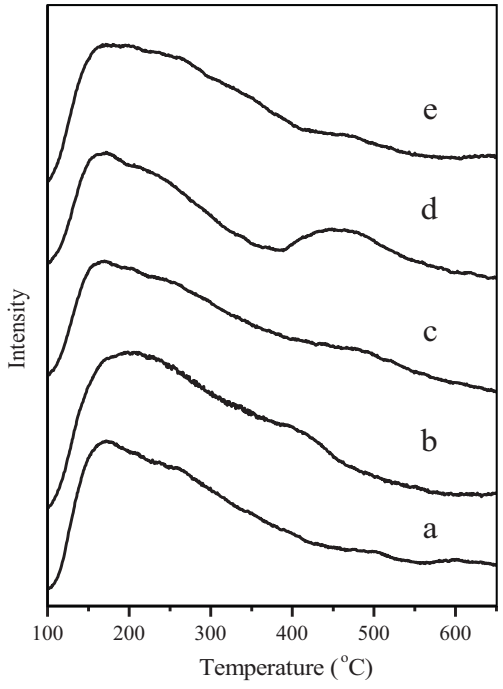

Fig. 3. NH$_3$-TPD profiles of (a) Pt–HSiW/ZrO$_2$, (b) Pt–LiSiW/ZrO$_2$, (c) Pt–KSiW/ZrO$_2$, (d) Pt–RbSiW/ZrO$_2$ and (e) Pt–CsSiW/ZrO$_2$.

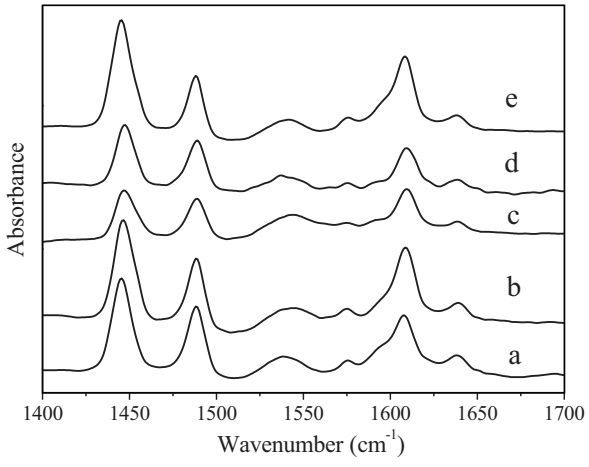

Fig. 4. FTIR spectra of pyridine adsorption of (a) Pt–HSiW/ZrO$_2$, (b) Pt–LiSiW/ZrO$_2$, (c) Pt–KSiW/ZrO$_2$, (d) Pt–RbSiW/ZrO$_2$ and (e) Pt–CsSiW/ZrO$_2$.

[34]. As listed in Table 1, in comparison with Pt–HSiW/ZrO_2, Pt–LiSiW/ZrO_2 and Pt–CsSiW/ZrO_2 even showed enhanced Brønsted and Lewis acid sites, while the concentration of Brønsted and Lewis acid sites declined significantly over Pt–KSiW/ZrO_2 and Pt–RbSiW/ZrO_2, particular for Lewis acid sites. It can be reasonably speculated that the remarkable increase of Lewis acid sites over Pt–LiSiW/ZrO_2 and Pt–CsSiW/ZrO_2 can be related to the alkaline metals exchange with HSiW, originating from the weakening/distortion of strong interaction between HSiW with support. The total acidity determined by Py-IR decreased in an order of Pt–LiSiW/ZrO_2 > Pt–CsSiW/ZrO_2 > Pt–HSiW/ZrO_2 > Pt–KSiW/ZrO_2 > Pt–RbSiW/ZrO_2, consistent well with the trend from NH_3-TPD results.

3.2. Catalytic performance

The catalytic performances at various reaction temperatures for glycerol hydrogenolysis over different catalysts are presented in Fig. 5. Raising reaction temperature has a positive influence on the glycerol conversion. As expected, glycerol activity improved progressively with the raising reaction temperature from 160 to 220 °C in all reaction temperatures. Activity of these catalysts decreased in the following order of Pt–LiSiW/ZrO_2 > Pt–CsSiW/ZrO_2 > Pt–HSiW/ZrO_2 > Pt–KSiW/ZrO_2 > Pt–RbSiW/ZrO_2 in all cases. Among them, Pt–LiSiW/ZrO_2 achieved the highest glycerol conversion up to 96.8% at 220 °C, while the conversion of Pt–RbSiW/ZrO_2 was as low as 61.7% under identical conditions. Regarding the selectivity, the increase of reaction temperature resulted in moderate enhancement of 1,3-PDO selectivity, but further increase led to distinct decrease of 1,3-PDO selectivity over all catalysts. Gong et al. [15] proposed that a reaction temperature higher than 180 °C can activate more terminal hydroxyl groups of glycerol. The obtained product distribution over these catalysts also showed that 1,2-PDO selectivity increased with the increasing temperature. Furthermore, the enhancement of temperature facilitates to promote sequential hydrogenolysis of propanediols (1,3-PDO + 1,2-PDO) to form propanols (1-PO + 2-PO), as described previously [12]. The degradation products methanol, ethanol and ethylene glycol are also favorable at higher temperature because of the excessive C—C bond cleavage. Based on above results, it can be inferred that alkaline metals modification has a dramatic effect on the catalytic performance of glycerol hydrogenolysis, particularly for the product distributions.

The representative glycerol conversion and main products selectivity of these catalysts at 180 °C are listed in Table 3. The addition of Li and Cs to Pt–HSiW/ZrO_2 enhanced the activity and 1,3-PDO selectivity appreciably, while K and Rb modified catalysts declined the reactivity. Among them, Pt–LiSiW/ZrO_2 performed best and reached 53.6% 1,3-PDO selectivity and 43.5% glycerol conversion at 180 °C. In comparison to other alkaline metals, the preference for Li modified HPAs as active acid component employed in various catalytic reactions has been reported

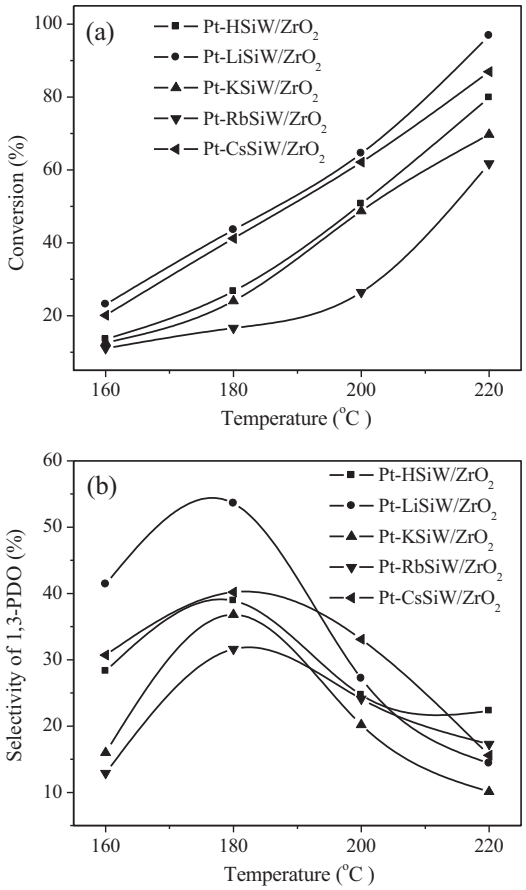

Fig. 5. Effect of reaction temperature on glycerol conversion (a) and 1,3-PDO selectivity (b) over different catalysts. Reaction conditions: 5.0 MPa, H_2/glycerol = 137:1 (molar ratio), WHSV = 0.09 h^{-1}.

owing to the enhanced dispersion and acidity, such as in glycerol dehydration [27]. Concurrently, the 1,2-PDO selectivity increased distinctly at the expense of propanols when alkaline metals were added, suggesting that alkaline metals modification suppressed the sequential hydrogenolysis of propanediols. Compared to previous reported catalysts, the 1,3-PDO yield of Pt–LiSiW/ZrO_2 is higher than that of Pt/WO_3/TiO_2/SiO_2 [15], Pt–Re/C [35], Rh–Re/SiO_2 [36], Rh/C + H_2WO_4 [14] and Ru/C + Amberlyst [37], despite employing relatively mild reaction conditions. Nonetheless, Tomishige and co-workers [17,18] reached better yield of 1,3-PDO over Ir–ReO_x/SiO_2 catalyst in a batch reactor, but under higher H_2 pressure (8 MPa) and using liquid H_2SO_4 as co-catalyst.

Pt particle size can have a direct impact on the hydrogenolysis activity where the presence of nanoscale Pt particles has been deemed essential for the superior activity. Our recent work [28] demonstrated that there was a good relationship between Pt

Table 3
Catalytic performance of glycerol hydrogenolysis over Pt–HSiWZrO_2 and alkaline metals modified catalysts at 180 °C.

Catalyst	Conversion (%)	Selectivity (%)[a]				
		1,3-PDO	1,2-PDO	1-PO	2-PO	Others[b]
Pt–HSiW/ZrO_2	26.7	38.9	9.2	39.9	3.6	8.4
Pt–LiSiW/ZrO_2	43.5	53.6	14.2	24.1	2.4	5.7
Pt–KSiW/ZrO_2	24.0	36.8	22.0	27.4	3.5	10.3
Pt–RbSiW/ZrO_2	16.6	31.6	25.4	28.9	4.0	10.1
Pt–CsSiW/ZrO_2	41.2	40.2	20.5	30.2	3.1	6.0

Reaction conditions: 180 °C, 5.0 MPa, H_2/glycerol = 137:1 (molar ratio), WHSV = 0.09 h^{-1}.
[a] 1,3-PDO, 1,3-propanediol; 1,2-PDO, 1,2-propanediol; 1-PO, 1-propanol; 2-PO, 2-propanol.
[b] Others: ethylene glycol, ethanol, methanol, and so on.

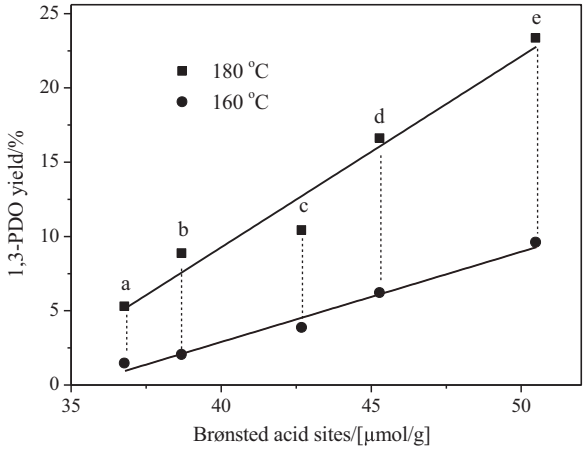

Fig. 6. Correlation between the amount of Brønsted acids sites and 1,3-PDO yield obtained at 160 °C and 180 °C over (a) Pt–RbSiW/ZrO_2, (b) Pt–KSiW/ZrO_2, (c) Pt–HSiW/ZrO_2, (d) Pt–CsSiW/ZrO_2 and (e) Pt–LiSiW/ZrO_2.

particle size and catalytic behavior of supported Pt–HSiW catalysts with different supports in glycerol hydrogenolysis; the superior activity of Pt–HSiW/ZrO_2 was primarily ascribed to smaller Pt particle size. However, this interpretation cannot be applied in the present work, for these Pt nanoparticles in all catalysts did not change obviously in size when alkaline metals were introduced, as indicated by CO-chemisorption. Additionally, the acidity of catalyst is also an important parameter in glycerol hydrogenolysis based on the dehydration–hydrogenation bi-functional mechanism. The catalytic activity dependence on acidity for glycerol hydrogenolysis over metal–acid bi-functional catalysts has been studied extensively. Balaraju et al. [10] have investigated glycerol hydrogenolysis over Ru/C catalysts using various solid acids as co-catalysts; there was a linear correlation between glycerol conversion and total acidity. Similar behavior has also been reported in the cases of Pt/WO_3/TiO_2/SiO_2 [15], Pt–sulfated zirconia [16] and Pt–HPAs/ZrO_2 [19]. Therefore, the promotional effect of Li and Cs modification on Pt–HSiW/ZrO_2 for glycerol hydrogenolysis could be explained by the improved acidity. With the increase of surface acid sites, more 3-HPA which is produced by the dehydration of glycerol molecules can be obtained. Subsequently, the formed 3-HPA on acid sites can be rapidly supplied to the nearby Pt sites for hydrogenation. As shown in Table 1 and Fig. 5, it can be observed that glycerol conversion increased gradually with the increasing acidity. The improved glycerol conversion with increase in acidity demonstrated that glycerol hydrogenolysis proceeded via dehydration of glycerol on acid sites and subsequent hydrogenation on metal center. Among these catalysts tested, the Pt–LiSiW/ZrO_2 catalyst gave the maximum glycerol conversion due to the most acid sites, as evidenced by NH_3-TPD and Py-IR. The above results confirmed that the activity of heteropolyacid can be adjusted by alkaline metals modification which can be instrument in determining the acidity by strengthening the mobility of available protons despite with reduced total number of protons.

Besides, the nature of acid sites can affect catalytic performance considerably. Brønsted acid sites can protonate the secondary hydroxyl group of glycerol, which finally hydrogenates to the formation of 1,3-PDO. Oh et al. [16] found that 1,3-PDO yield was approximately proportional to the concentration of Brønsted acid sites and proposed that Brønsted acid sites preferentially generated 1,3-PDO. Thus, as shown in Fig. 5 and Table 1, the Pt–LiSiW/ZrO_2 catalyst reached the highest yield of 1,3-PDO, which was attributed to the most Brønsted acid sites, as deduced from Py-IR. As presented in Fig. 6, a linear relationship between 1,3-PDO yield at 160 °C or 180 °C and the concentration of Brønsted acid sites can be derived, which is a new direct evidence that Brønsted acid sites are indispensable for the selective production of 1,3-PDO from glycerol hydrogenolysis. Specifically, the hydrogenolysis of glycerol to 1,3-PDO included two steps, the dehydration of secondary C—O bond of glycerol to form 3-HPA on Brønsted acid sites and subsequent hydrogenation to produce 1,3-PDO on metal sites. Though several reports [13,37] claimed that the dehydration of secondary C—O bond of glycerol proceeded on the metal surface, it did not seem plausible in this case as the number of accessible surface Pt sites were almost the same over these catalysts while 1,3-PDO yield were remarkably different. Consequently, the dehydration of glycerol is supposed to occur on Brønsted acid sites. This chemistry is consistent well with that proposed by Alhanash et al. [38] who showed that the secondary C—O bond of glycerol dehydration occurred on Brønsted acid sites over $Cs_{2.5}H_{0.5}PW_{12}O_{40}$ whereas the primary C—O bond of glycerol dehydration proceeded on Lewis acid sites over Zn–Cr mixed oxide.

3.3. Reaction mechanism

Indeed the underling reaction mechanism about the secondary C—O bond hydrogenolysis of glycerol to 1,3-PDO is subject to some debate that it proceeds via direct substitution of secondary C—O bond by incoming hydrogen or bifunctional process of dehydration–hydrogenation. In the presence of Ir–ReO_x/SiO_2 using H_2SO_4 as co-catalyst, Tomishige and co-workers [17,18,39] proposed direct reaction mechanism for the formation of 1,3-PDO from glycerol via 2,3-dihydroxypropoxide species. Dumesic and co-workers [32] have systematically investigated reaction mechanism for polyols hydrogenolysis over ReO_x-promoted Rh/C catalyst; the observed reactivity trends and results from theoretical calculation were indications of bifunctional process involving acid-catalyzed dehydration coupled with metal-catalyzed hydrogenation. It seems apparently that both provide plausible reaction processes which highly relate to the catalytic system and operation conditions. According to the direct reaction mechanism, the acid component did not directly involve in the reaction cycle and affect 1,3-PDO selectivity. Contrarily, in our reaction system the enhanced acidity (particularly for Brønsted acid sites) promoted glycerol hydrogenolysis and 1,3-PDO selectivity significantly. The linear relationship between 1,3-PDO yield and concentration of Brønsted acid sites presented clear evidence for its essential role in the selective hydrogenolysis of glycerol to 1,3-PDO under our reaction system. Moreover, our previous report [19] showed that pure Lewis acid catalyst Pt/ZrO_2 exhibited high 1,2-PDO selectivity while very poor 1,3-PDO selectivity under similar conditions, arguing that Lewis acid sites cannot be responsible for the 1,3-PDO formation. Thus, the secondary C—O bond hydrogenolysis of glycerol to 1,3-PDO in our reaction chemistry proceeded most probably via dehydration of glycerol on Brønsted acid sites followed by hydrogenation on nearby Pt sites. Nevertheless, the dehydration product 3-HPA was not detected in the product mixture. Oh et al. [16] have disclosed that 3-HPA is highly active over Pt based catalyst and can undergo hydrogenation to produce 1,3-PDO rapidly. Thus, to corroborate this point further, an additional experiment of glycerol dehydration was conducted using Pt–free LiSiW/ZrO_2 catalyst under the similar conditions as glycerol hydrogenolysis. 3-HPA was still not detected and the dominant product was acrolein derived from consecutive dehydration of 3-HPA [40]. Similar product distributions have been obtained in the cases of CsPW and LiSiW/SiO_2 in glycerol dehydration [27,38]. The 3-HPA can convert to acrolein in the absence of Pt based catalyst, indicating that though 3-HPA is probably a dehydration intermediate, subsequent conversion to 1,3-PDO requires a metal hydrogenation center that is not provided by LiSiW/ZrO_2 or other acid components alone.

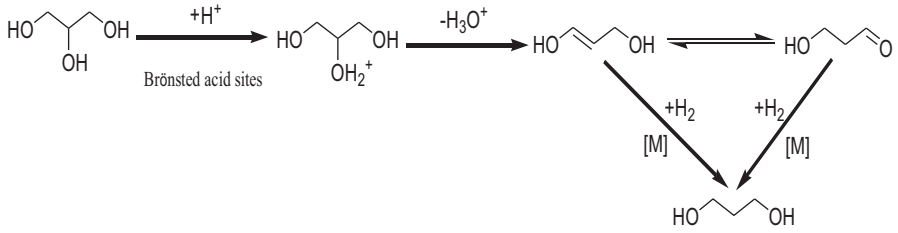

Scheme 1. The proposed reaction mechanism for glycerol hydrogenolysis to 1,3-propanediol.

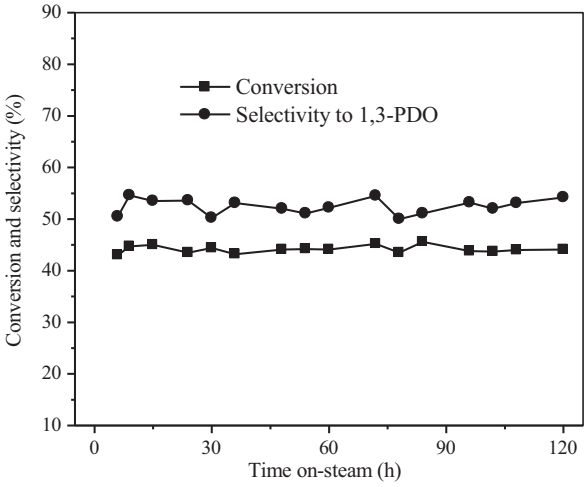

Fig. 7. Long-term performance of Pt–LiSiW/ZrO_2 in glycerol hydrogenolysis. Reaction conditions: 180 °C, 5.0 MPa, H_2/glycerol = 137:1 (molar ratio), WHSV = 0.09 h^{-1}.

Recently, the quantum mechanical calculations [41] for glycerol dehydration over acidic H-ZSM-5 zeolite revealed that the close contact of glycerol secondary C—O bond with zeolite Brønsted acid proton can significantly lengthen and impair the C—O bond. Consequently, the protonation of glycerol by Brønsted acid site can promote glycerol dehydration. The in situ FTIR indicated that the intermediate of secondary C—O bond of glycerol dehydration was 3-HPA which was originated from tautomerization reaction of 1,3-dihydroxypropene [42]. Subsequently, the yielded 3-HPA can proceed hydrogenation rapidly under hydrogen atmosphere over Pt-based catalyst. Based on the above discussions and our experimental results, a possible mechanistic scheme was proposed in Scheme 1 to explain the role of Brønsted acid sites for the selective formation of 1,3-PDO. Initially, the adsorbed glycerol is protonated by Brønsted acid sites at secondary hydroxyl group, which will further weaken the secondary C—O bond and promote the removal of secondary hydroxyl group as a water molecule [38,41]. Accompanying by the elimination of water molecule, 1,3-dihydroxypropene is generated on the catalyst surface, which can proceed tautomerization reaction to its keto-form 3-HPA. Both of them can further hydrogenate to produce 1,3-PDO on nearby active metal sites.

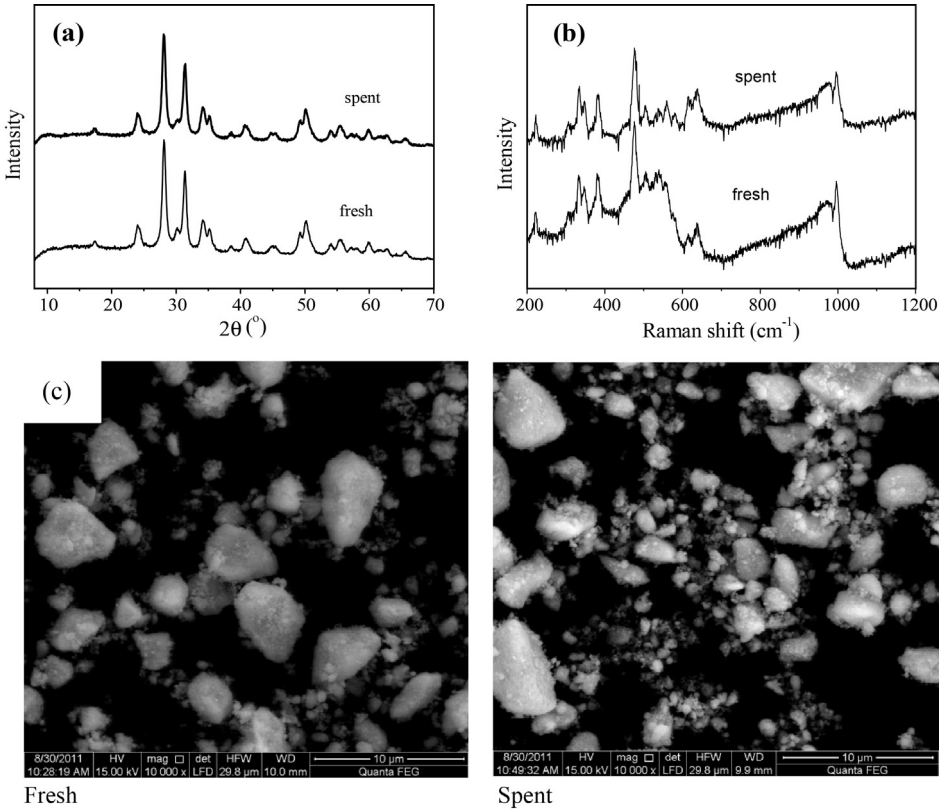

Fig. 8. Characterization results of fresh and spent Pt–LiSiW/ZrO_2 catalysts (a) XRD; (b) Raman; (c) SEM images.

3.4. Long-term performance of Pt–LiSiW/ZrO_2

Since Pt–LiSiW/ZrO_2 catalyst presented the best 1,3-PDO selectivity, the long-term performance over this sample was conducted to explore the stability at 180 °C. For comparison, the long-term performance of Pt–HSiW/ZrO_2 was also tested while this catalyst deactivated rapidly after 72 h time-on-stream due to the leaching of HSiW component. As illustrated in Fig. 7, the Pt–LiSiW/ZrO_2 catalyst did not present any distinct loss in the activity within 120 h time-on-stream, despite in the harsh reaction conditions. Concurrently, the product distribution did not show obvious fluctuation during the complete test. This could indicate that the Pt–LiSiW/ZrO_2 catalyst was rather robust under these conditions, which can be further confirmed by a series of characterization techniques including ICP, XRD, Raman, CO-chemisorption, as well as SEM.

These characterization results for the fresh and spent samples provide clear clues concerning the high stability of Pt–LiSiW/ZrO_2. As displayed in Fig. 8a, both the fresh and spent samples presented similar XRD diffraction patterns, suggesting the intact structure during the reaction. Similar Raman spectra (Fig. 8b) between the fresh and spent ones also demonstrated the fine preservation of HSiW Keggin structure on the support surface. Haider et al. [30] claimed that the binding strength of partially doped HSiW was crucial to remain Keggin structure and acidity of active components that determined the origin of the long-term stability. As indicated by SEM (Fig. 8c), the spent sample showed the similar morphology as fresh one because of good hydrothermal stability of support ZrO_2, in well agreement with previous literature [28]. On the other hand, alkaline metal Li modification can probably improve the water-tolerant property and reduce the leaching of active components, as indicated by ICP test. In addition, the Pt species was not sintered in a 120 h test, as determined by CO-chemisorption. In sum, the superior stability of Pt–LiSiW/ZrO_2 lies in the strong interaction of active components with support ZrO_2, remaining of unique Keggin structure and improved water–tolerance property stemmed from successful incorporation Li^+ into HSiW Keggin structure.

4. Conclusions

In this work, addition of alkaline metals Li, K, Rb and Cs has proved to be a powerful approach to tune the acidic property of HSiW in terms of Brønsted acid sites and Lewis acid sites and to control the catalytic performance in glycerol hydrogenolysis. Among them, Pt–LiHSiW/ZrO_2 promoted the reactivity most pronouncedly due to the enhanced Brønsted acid sites, attaining 43.5% glycerol conversion with 53.6% 1,3-PDO selectivity at 180 °C and 5 MPa. Additionally, this catalyst exhibited superior long-term performance as well as holding robust structure, as evidenced by ICP, XRD, Raman, CO-chemisorption and SEM.

There is a linear relationship between 1,3-PDO yield and concentration of Brønsted acid sites determined by Py-IR. New direct evidence has been provided regarding the nature of acid sites required for the selective hydrogenolysis of glycerol to 1,3-PDO, which supports the importance of Brønsted acid sites for this reaction. A reaction mechanism has been proposed to elucidate the role of Brønsted acid sites in glycerol secondary C—O bond cleavage. Therefore, in order to obtain high yield of 1,3-PDO, it is desirable to design new catalyst with large amount of Brønsted acid sites.

Acknowledgements

The authors gratefully acknowledge financial support of the National Natural Science Foundation of China (No. 20976185) and the Major State Basic Research Development Program of China (973 Program) (No. 2012CB215305).

References

[1] A. Corma, S. Iborra, A. Velty, Chemical Reviews 107 (2007) 2411–2502.
[2] G.W. Huber, S. Iborra, A. Corma, Chemical Reviews 106 (2006) 4044–4098.
[3] M. Pagliaro, R. Ciriminna, H. Kimura, M. Rossi, C. Della Pina, Angewandte Chemie International Edition 46 (2007) 4434–4440.
[4] Y. Nakagawa, K. Tomishige, Catalysis Science & Technology 1 (2011) 179–190.
[5] B. Katryniok, S. Paul, V. Belliere-Baca, P. Rey, F. Dumeignil, Green Chemistry 12 (2010) 2079–2098.
[6] C.H.C. Zhou, J.N. Beltramini, Y.X. Fan, G.Q.M. Lu, Chemical Society Reviews 37 (2008) 527–549.
[7] I. Jiménez-Morales, F. Vila, R. Mariscal, A. Jiménez-López, Applied Catalysis B: Environmental 117/118 (2012) 253–259.
[8] D.L. King, L. Zhang, G. Xia, A.M. Karim, D.J. Heldebrant, X. Wang, T. Peterson, Y. Wang, Applied Catalysis B: Environmental 99 (2010) 206–213.
[9] A. Iriondo, J.F. Cambra, V.L. Barrio, M.B. Guemez, P.L. Arias, M.C. Sanchez-Sanchez, R.M. Navarro, J.L.G. Fierro, Applied Catalysis B: Environmental 106 (2011) 83–93.
[10] M. Balaraju, V. Rekha, P.S.S. Prasad, B.L.A.P. Devi, R.B.N. Prasad, N. Lingaiah, Applied Catalysis A – General 354 (2009) 82–87.
[11] S. Zhu, Y. Zhu, S. Hao, L. Chen, B. Zhang, Y. Li, Catalysis Letters 142 (2012) 267–274.
[12] L.-Z. Qin, M.-J. Song, C.-L. Chen, Green Chemistry 12 (2010) 1466–1472.
[13] T. Kurosaka, H. Maruyama, I. Naribayashi, Y. Sasaki, Catalysis Communications 9 (2008) 1360–1363.
[14] J. Chaminand, L. Djakovitch, P. Gallezot, P. Marion, C. Pinel, C. Rosier, Green Chemistry 6 (2004) 359–361.
[15] L. Gong, Y. Lu, Y. Ding, R. Lin, J. Li, W. Dong, T. Wang, W. Chen, Applied Catalysis A – General 390 (2010) 119–126.
[16] J. Oh, S. Dash, H. Lee, Green Chemistry 13 (2011) 2004–2007.
[17] Y. Nakagawa, Y. Shinmi, S. Koso, K. Tomishige, Journal of Catalysis 272 (2010) 191–194.
[18] Y. Amada, Y. Shinmi, S. Koso, T. Kubota, Y. Nakagawa, K. Tomishige, Applied Catalysis B: Environmental 105 (2011) 117–127.
[19] S. Zhu, Y. Qiu, Y. Zhu, S. Hao, H. Zheng, Y. Li, Catalysis Today (2012), http://dx.doi.org/10.1016/j.cattod.2012.09.011.
[20] M. Misono, Catalysis Today 144 (2009) 285–291.
[21] I.V. Kozhevnikov, Journal of Molecular Catalysis A: Chemical 305 (2009) 104–111.
[22] P. Ferreira, I.M. Fonseca, A.M. Ramos, J. Vital, J.E. Castanheiro, Applied Catalysis B: Environmental 98 (2010) 94–99.
[23] S. Zhu, Y. Zhu, X. Gao, T. Mo, Y. Zhu, Y. Li, Bioresource Technology 130 (2013) 45–51.
[24] C.F. Oliveira, L.M. Dezaneti, F.A.C. Garcia, J.L. de Macedo, J.A. Dias, S.C.L. Dias, K.S.P. Alvim, Applied Catalysis A – General 372 (2010) 153–161.
[25] L. Pesaresi, D.R. Brown, A.F. Lee, J.M. Montero, H. Williams, K. Wilson, Applied Catalysis A – General 360 (2009) 50–58.
[26] K. Narasimharao, D.R. Brown, A.F. Lee, A.D. Newman, P.F. Siril, S.J. Tavener, K. Wilson, Journal of Catalysis 248 (2007) 226–234.
[27] H. Atia, U. Armbruster, A. Martin, Applied Catalysis A – General 393 (2011) 331–339.
[28] S. Zhu, Y. Zhu, S. Hao, H. Zheng, T. Mo, Y. Li, Green Chemistry 14 (2012) 2607–2616.
[29] H. Atia, U. Armbruster, A. Martin, Journal of Catalysis 258 (2008) 71–82.
[30] M.H. Haider, N.F. Dummer, D. Zhang, P. Miedziak, T.E. Davies, S.H. Taylor, D.J. Willock, D.W. Knight, D. Chadwick, G.J. Hutchings, Journal of Catalysis 286 (2012) 206–213.
[31] I. Gandarias, P.L. Arias, J. Requies, M.B. Guemez, J.L.G. Fierro, Applied Catalysis B: Environmental 97 (2010) 248–256.
[32] M. Chia, Y.J. Pagaĭn-Torres, D. Hibbitts, Q. Tan, H.N. Pham, A.K. Datye, M. Neurock, R.J. Davis, J.A. Dumesic, Journal of the American Chemical Society 133 (2011) 12675–12689.
[33] K.T.V. Rao, P.S.S. Prasad, N. Lingaiah, Green Chemistry 4 (2012) 1507–1514.
[34] P. Lauriol-Garbey, G. Postole, S. Loridant, A. Auroux, V. Belliere-Baca, P. Rey, J.M.M. Millet, Applied Catalysis B: Environmental 106 (2011) 94–102.
[35] O.M. Daniel, A. DeLaRiva, E.L. Kunkes, A.K. Datye, J.A. Dumesic, R.J. Davis, Chemcatchem 2 (2010) 1107–1114.
[36] Y. Shinmi, S. Koso, T. Kubota, Y. Nakagawa, K. Tomishige, Applied Catalysis B: Environmental 94 (2010) 318–326.
[37] T. Miyazawa, Y. Kusunoki, K. Kunimori, K. Tomishige, Journal of Catalysis 240 (2006) 213–221.
[38] A. Alhanash, E.F. Kozhevnikova, I.V. Kozhevnikov, Applied Catalysis A – General 378 (2010) 11–18.
[39] S. Koso, H. Watanabe, K. Okumura, Y. Nakagawa, K. Tomishige, Applied Catalysis B: Environmental 111–112 (2012) 27–37.
[40] Y.T. Kim, K.-D. Jung, E.D. Park, Applied Catalysis B: Environmental 107 (2011) 177–187.
[41] K. Kongpatpanich, T. Nanok, B. Boekfa, M. Probst, J. Limtrakul, Physical Chemistry Chemical Physics 13 (2011) 6462–6470.
[42] E. Yoda, A. Ootawa, Applied Catalysis A – General 360 (2009) 66–70.